Article

Removal of Pb(II) from Acid Mine Drainage with Bentonite-Steel Slag Composite Particles

Xinhui Zhan [1],*[ID]**, Liping Xiao** [2] **and Bing Liang** [3]

[1]   School of Mines, Liaoning Technical University, Fuxin 123000, China
[2]   School of Civil Engineering, Liaoning Technical University, Fuxin 123000, China
[3]   School of Mechanics and Engineering, Liaoning Technical University, Fuxin 123000, China
*   Correspondence: zxhzhanxinhui@163.com

check for updates

Abstract: Abandoned lead and zinc (Pb-Zn) mines around the world produce large amounts of acid mine drainage (AMD) containing Pb(II), which is toxic and accumulates in the environment and in living organisms. Bentonite-steel slag composite particles (BSC) are a new type of acid mine drainage (AMD) treatment material that can remove heavy metal ions and reduce acidity. To date, there have been no reports on the treatment of Pb(II)-containing AMD using BSC. Therefore, the effects of pH, reaction time, temperature, and Pb(II) concentration on the adsorption of Pb(II) onto BSC were studied. Moreover, the BSC before and after the reaction, as well as the precipitation after the reaction, were characterized by scanning electron microscopy and X-ray diffraction analyses. The effect of pH on the adsorption process is similar to that of the formation of soluble and insoluble hydrolysates of Pb(II) on pH. The adsorption mechanism includes ion exchange, complexation, precipitation, and synergistic adsorption–coagulation effect. Adsorption kinetics are best-fit with the pseudo-second order kinetics model ($R^2 > 0.98$). Furthermore, the total adsorption rate is controlled by liquid film diffusion and in-particle diffusion, the liquid film diffusion rate being higher than the in-particle diffusion rate. The isothermal adsorption of Pb(II) onto BSC fit well with Langmuir and Brunauer Emmett Teller (BET) isotherms ($R^2 > 0.995$), and both single layer adsorption and local multilayer adsorption were observed. Thermodynamic analysis revealed that the adsorption process is spontaneous and endothermic, and that the degree of freedom increases with time. In summary, this study provides a theoretical basis for the use of BSC in treating AMD containing Pb(II).

Keywords: adsorption-coagulation; bentonite-steel slag composite particles (BSC); isotherms; kinetics; Pb(II); thermodynamics

1. Introduction

Acid mine drainage (AMD) is an inevitable by-product of mining production in the case of the occurrence of sulfide minerals [1,2]. AMD is highly acidic and contains high concentrations of toxic substances, including heavy metal ions [3,4]. Consequently, the discharge of untreated AMD into natural water receivers can cause significant damage to aquatic flora and fauna [5,6]. In addition, groundwater pollution due to AMD is a serious problem too. To mitigate the negative effects of AMD on ecosystems and human health, several treatment approaches have been developed, including neutralization precipitation [7], electrochemical [8], membrane separation [9,10], microbial treatment [11,12], constructed wetland [13], and adsorption [14] methods. Among these, the neutralization precipitation and adsorption methods [15,16] are widely used.

Traditionally, AMD is neutralized using lime. However, when lime neutralizes wastewater, the generated metal hydroxide has a low specific gravity and can be easily broken into small particles when strongly stirred or transported. Therefore, its sedimentation rate is very low and solid-liquid

separation is difficult. The treatment process is complex and involves several stages including the use of flocculant, adsorbent, and a filtration process, whereas on the same time the neutralized sludge produced is voluminous and difficult to dispose. Activated carbon [17,18] is commonly used for adsorption and has become a standard adsorbent for urban and industrial wastewater recycling; however, owing to its high cost, the production of low-cost substitutes for activated charcoal has become a hot topic for research. These low-cost adsorbent substitutes for heavy metal adsorption range from natural materials to industrial and agricultural by-products such as red mud [19], coffee grounds [20], bentonite [21], silicate [22], zeolite [23], fly ash [24], moss [25], tea residue [26], and peanut shells [27].

Bentonite is a good substitute for activated carbon. It is a clay with montmorillonite as its primary component [28,29]. Montmorillonite is a type of 2:1 layered silicate composed of a layer of alumino-oxygen octahedra sandwiched between two layers of silica-oxygen tetrahedra. Because of lattice displacement, electronegativity, and ion exchange in montmorillonite as well as its large surface area, bentonite has a strong ability to adsorb metal cations [30]. Moreover, bentonite is an inexpensive and excellent mineral with abundant reserves in China and can be used to remove metal cations in AMD. However, it cannot neutralize acid. Steel slag is a type of metallurgical by-product, whose main phase is calcium glass. As a solid waste, steel slag recycling and utilization contributes to environmental pollution. Due to mineral compositions such as calcium glass, steel slag can release alkalinity in aqueous solution [31–33], which can be used to neutralize AMD acidity.

Our research group developed a new adsorbent named bentonite–steel slag composite particles (BSC) [34]. These particles benefit from the excellent adsorption potential of bentonite for heavy metal cations and the ability of steel slag to release alkalinity, which neutralizes acid, thereby precipitating heavy metal ions. In addition, these composite particles induce a synergistic adsorption–coagulation effect that aids the removal of heavy metal ions. Thus, BSC can be used as a viable adsorbent alternative to the combination of expensive activated carbon or ion exchange resins and lime. In particular, BSC particles utilize solid waste, significantly reduce the processing cost for AMD processing, and allow solids and liquids to be easily separated; in summary, BSC is a new, multifunctional mineral material that allows for neutralization, adsorption, coagulation, and filtration.

Lead and zinc (Pb-Zn) mines are quite common worldwide; while approximately 240 mines are active, the majority of these mines have been abandoned for decades [5]. Abandoned mining wastes represent a serious environmental hazard and can form AMD containing Pb(II) and Zn(II). The harm of AMD containing Pb(II) is much greater than that of AMD containing Fe(II), Mn(II), Cu(II), and Zn(II). Pb is toxic and accumulates in the environment and in organisms. When excessive Pb accumulates in the human body, it can severely damage the circulatory, nervous, gastrointestinal, and excretory systems as well as other tissue systems [35–37]. Development of novel low-cost adsorbents for heavy metals removal has attracted significant research attention. Liu et al. studied the adsorption performance of Pb(II) ions from aqueous solutions onto a novel complex of coffee grounds and attapulgite clay [20]. Li et al. studied the removal of Pb(II) and Cr(VI) ions by amino-modified nano-sized illite-smectite clay [21]. Sun et al. constructed nanostructured silicates on diatomite for Pb(II) and Cd(II) removal [22]. Yuan et al. prepared Fe2O3-ceramicite (FOC) by sintering bentonite, iron powder (IP), and activated carbon (AC) at 1073 K, which has a good adsorption properties for Pb(II) in AMD [36]. However, most of these reported adsorbents only have the function of removing Pb(II) and cannot neutralize AMD acidity. Thus far, there have been no studies on the treatment of AMD containing Pb(II) by using BSC. Thus, in this study, BSC was tested as an adsorbent to treat acidic wastewater containing Pb(II). In particular, the kinetic, isothermal adsorption, and thermodynamic properties between BSC and Pb(II), as well as the adsorption mechanism between them were studied. Furthermore, the BSC before and after the reaction, as well as the precipitation after the reaction were characterized by scanning electron microscopy (SEM) and X-ray diffraction (XRD) analyses. In addition, the effects of pH, reaction time, initial Pb(II) concentration, and temperature on BSC adsorption were discussed. Herein we studied in

detail the removal behavior, influencing factors and removal mechanism of Pb(II) in AMD by a new adsorbent BSC, providing a theoretical basis for the treatment of Pb(II)-containing AMD by using BSC.

2. Materials and Methods

2.1. Materials

Na-bentonite (<74 µm, Jin Shi bentonite mining co., Ltd. in Fuxin City, Liaoning Province, China), steel slag (<74 µm, Zhong Tian Steel Plant in Fuxin City, Liaoning Province, China) and Na_2CO_3 (Xilong Chemical, Shenyang, China) were used as raw materials for BSC preparation. The chemical compositions of the bentonite sample and steel slag are listed in Tables 1 and 2, respectively. An appropriate amount of $Pb(NO_3)_2$ (Xilong Chemical, Shenyang, China) was dissolved in deionized water (DW) to obtain a 1 g L^{-1} stock solutions of Pb(II), which was then diluted with more DW to obtain the desired concentration of Pb(II) in solution. The pH of the initial solution (pH_0) was maintained between 3.0–5.0 by adding 0.1 M HNO_3 or 0.1 M NaOH solution. Before use, all the conical flasks were immersed in 0.1 M HNO_3 solution for 24 h and then rinsed with DW three times. All the chemicals used in this study were of analytical grade.

Table 1. Chemical composition of the bentonite sample.

Constituent	Mass Percentage (%)
SiO_2	71.39
Al_2O_3	14.4
Na_2O	1.98
Fe_2O_3	1.71
MgO	1.52
CaO	1.20
K_2O	0.44
TiO_2	<0.1

Table 2. Chemical composition of the steel slag.

Constituent	Mass Percentage (%)
Fe_2O_3	38.83
CaO	32.73
SiO_2	12.33
MgO	10
MnO	3.29
P_2O_5	1.12
Al_2O_3	0.18

2.2. Preparation of BSC

Bentonite and steel slag powder were mixed in a ratio of 1:1, and 5% of total mass Na_2CO_3 was added. After the mixture was evenly mixed, an appropriate amount of DW was added, and the mixture was stirred; then, composite particles with a particle size of 2 mm were prepared using an extrusion granulator. The particles were aged for 12 h in a dark, ventilated location; then, they were heated in a crucible in a preheated muffle furnace at temperatures of 523 K to 773 K for 60 min. After roasting, the particles were allowed to cool naturally to obtain the adsorbent. The chemical compositions and physical properties of BSC are listed in Table 3.

Table 3. Chemical composition and physical properties of BSC.

Constituent	Mass Percentage (%)
SiO_2	43.34
Al_2O_3	7.83
CaO	17.54
MgO	5.42
MnO	2.73
P_2O_5	0.69
Na_2O	1.42
K_2O	0.19
Fe_2O_3	18.98
Surface area ($m^2 g^{-1}$)	130.6
pH_{pzc}	2.01

2.3. Effect of pH on Pb(II) Adsorption

A batch adsorption test was performed in a thermostated shaker (298.0 ± 0.5 K, 100 rpm). The BSC dosage was fixed as 10 g L^{-1}, while the initial solute concentration of Pb(II) was 100 mg L^{-1}. pH_0 was changed from 1 to 6.5 with increments of 0.5; in particular, pH_0 was adjusted by adding 0.1 M HNO_3 or 0.1 M NaOH solution. After allowing the reaction to continue for 24 h, the resulting equilibrium solution was filtered. The equilibrium concentration of the solution was determined using an atomic absorption spectrophotometer (AAS) (Hitachi Z-2000, Tokyo, Japan), while the equilibrium pH (pH_e) was determined using a glass electrode potentiometer.

2.4. Adsorption Kinetics

Kinetics experiments were conducted in a thermostated shaker (298 ± 0.5 K, 100 rpm). The BSC dosage was fixed at 10 g L^{-1}, while the initial solute concentrations of Pb(II) were 200 and 300 mg L^{-1}. The equilibration times were set between 5 to 540 min. Samples were extracted in a controlled temperature environment at different intervals and filtered. The concentration of Pb(II) in the filtrate was determined using the AAS.

2.5. Effects of Temperature and Solute Concentration

Batch tests were conducted to study Pb(II) adsorption at different temperatures and solution concentrations. The temperature range was from 278 to 318 K with increments of 10 K. The BSC dosage was fixed at 10 g L^{-1} with initial solute concentrations of 100, 200, 400, 500, and 600 mg L^{-1}. All samples were equilibrated for 24 h in a thermostated shaker at 100 rpm; then, the equilibrium Pb(II) concentrations were measured using the AAS to calculate the amount of Pb(II) adsorbed on the sorbent.

In order to ensure the reliability of our test results, two groups of batch tests were conducted in parallel and mean values were recorded; in addition, blank sample tests were conducted to test the initial concentration of Pb(II).

The adsorption amount at equilibrium q_e (mg g^{-1}) and removal efficiency R (%) of Pb(II) by BSC was calculated as follows:

$$q_e = \frac{(C_0 - C_e)V}{m}, \tag{1}$$

$$R = \frac{C_0 - C_e}{C_0} \times 100\%, \tag{2}$$

where C_0 and C_e are the initial and equilibrium solute concentration (mg L^{-1}), respectively, V is the volume of solution (L), and m is the quantity of BSC (g).

2.6. Microstructure Characterization

The surface microstructures of BSC before and after the reaction, as well as the precipitate after the reaction, were analyzed using a FEI Quanta 200 scanning electron microscope. The XRD-6100 X-ray diffractometer was used to conduct micro analysis of the pre-reaction BSC, post-reaction BSC, and mineral phase of the post-reaction precipitate. The diffraction angle ranged from 5° to 90°, and the scanning rate was 6°/min.

3. Results and Discussion

3.1. Effect of pH on Pb(II) Adsorption and Associated Mechanisms

From Figure 1, it can be observed that when the initial pH (i.e., pH_0) increased from 1 to 2, the Pb(II) removal rate increased from 39.44% to 99.98%, and the equilibrium pH (i.e., pH_e) increased from 1.55 to 8.36. In addition, when pH_0 was between 2 to 6.5, the Pb(II) removal rate approached 100%, while pH_e remained between 9 and 10. Thus, it is clear that if pH_0 is controlled between 2 to 6.5, BSC could effectively remove Pb(II) from the solution.
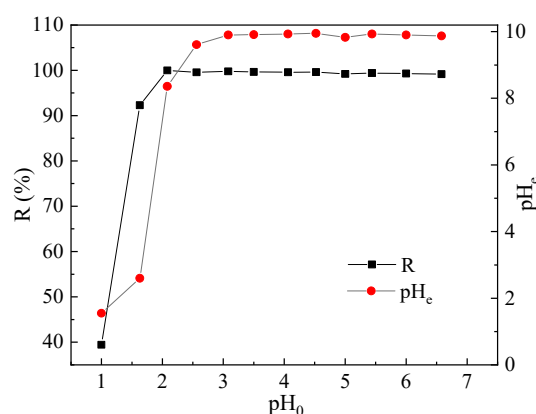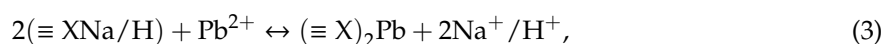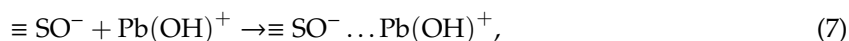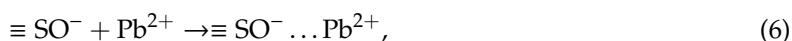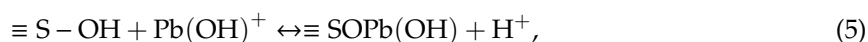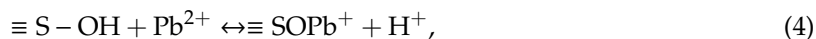

Figure 1. Effect of initial pH on the removal efficiency of BSC for Pb(II) and equilibrium pH for Pb(II) adsorption.

The lower the pH_0 of solution containing Pb(II), the more the H^+ ions in it. These H^+ ions would have competed with Pb(II) for adsorption; in particular, the adsorption sites on BSC would be occupied by a large number of H^+ ions, which would have impeded Pb(II) adsorption on BSC. Furthermore, because of the limited alkalinity release of BSC, the higher the number of H^+ ions in the solution, the more the OH^- ions that will be consumed by them, leading to a reduction in the number of OH^- ions that could form hydroxides with Pb(II), consequently weakening the precipitation removal effect of BSC on Pb(II). Therefore, when pH_0 was low, the removal rate was low.

Because BSC released alkalinity to regulate the pH of the solution, the pH of the solution changed constantly. It was observed that the effect of pH on adsorption process was similar to that of the formation of soluble and insoluble lead hydrolysates on the pH value [38]. In particular, when pH < 7, Pb(II) in the solution existed in the form of Pb^{2+}; therefore, the primary adsorption mechanism was ion exchange, i.e., H^+, Na^+, and Ca^{2+} ions on the exchangeable adsorption sites of BSC were replaced by Pb^{2+} ions. In contrast, when 7 < pH < 10, Pb(II) occurred in the form of $Pb(OH)^+$ and $Pb(OH)_2$; thus, the removal of Pb(II) by BSC included $Pb(OH)^+$ adsorption, complexation, and $Pb(OH)_2$ precipitation. Lastly, when pH > 10, $Pb(OH)_2$ and $Pb(OH)^{3-}$ were the main forms in which Pb(II) existed, and thus, the removal of Pb(II) by BSC was primarily due to $Pb(OH)_2$ precipitation.
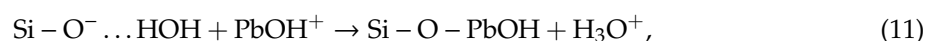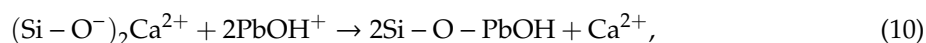
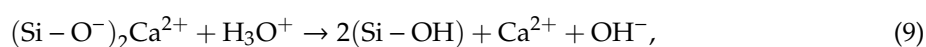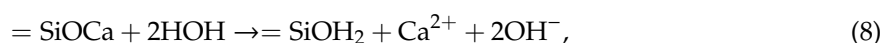The interaction of Pb(II) in solution with minerals [39,40] present in BSC can be expressed as follows:

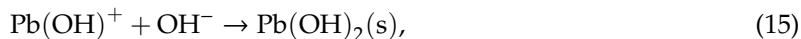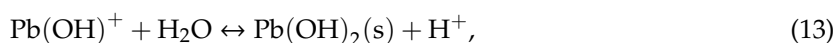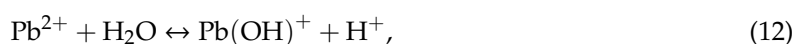$$2(\equiv XNa/H) + Pb^{2+} \leftrightarrow (\equiv X)_2 Pb + 2Na^+/H^+, \tag{3}$$

$$\equiv S - OH + Pb^{2+} \leftrightarrow \equiv SOPb^{+} + H^{+}, \tag{4}$$

$$\equiv S - OH + Pb(OH)^{+} \leftrightarrow \equiv SOPb(OH) + H^{+}, \tag{5}$$

$$\equiv SO^{-} + Pb^{2+} \rightarrow \equiv SO^{-}\ldots Pb^{2+}, \tag{6}$$

$$\equiv SO^{-} + Pb(OH)^{+} \rightarrow \equiv SO^{-}\ldots Pb(OH)^{+}, \tag{7}$$

where $\equiv S$ represents the adsorption site bonded with a hydroxyl group in BSC; $\equiv S - OH_2^{+}$, $\equiv S - OH$, and $\equiv S - O^{-}$ are protonated, neutral, and ionized hydroxyl groups, respectively; and $\equiv X$ represents the permanently charged site with a negative charge for cations.

Considering the nature of the steel slags in BSC, an exchange interaction of the slag glass [38] in solution can be expressed as follows:

$$= SiOCa + 2HOH \rightarrow= SiOH_2 + Ca^{2+} + 2OH^{-}, \tag{8}$$

$$(Si - O^{-})_2Ca^{2+} + H_3O^{+} \rightarrow 2(Si - OH) + Ca^{2+} + OH^{-}, \tag{9}$$

$$(Si - O^{-})_2Ca^{2+} + 2PbOH^{+} \rightarrow 2Si - O - PbOH + Ca^{2+}, \tag{10}$$

$$Si - O^{-}\ldots HOH + PbOH^{+} \rightarrow Si - O - PbOH + H_3O^{+}, \tag{11}$$

Furthermore, hydrolysis and precipitation could be expressed as follows:

$$Pb^{2+} + H_2O \leftrightarrow Pb(OH)^{+} + H^{+}, \tag{12}$$

$$Pb(OH)^{+} + H_2O \leftrightarrow Pb(OH)_2(s) + H^{+}, \tag{13}$$

$$Pb^{2+} + 2OH^{-} \rightarrow Pb(OH)_2(s), \tag{14}$$

$$Pb(OH)^{+} + OH^{-} \rightarrow Pb(OH)_2(s), \tag{15}$$

3.2. Effect of Contact Time and Adsorption Kinetics

Figure 2 shows the Pb(II) adsorption curve over time. It can be observed that a higher initial concentration of Pb(II) leads to a higher adsorption amount. This can be explained as follows: the higher the initial concentration of Pb(II), the greater the concentration gradient between BSC and water, the stronger the driving force experienced by ions to diffuse to the surface of the BSC particles, and more the number of ions removed via precipitation, leading to a larger adsorption amount. For further analysis, the experimental data were fitted using pseudo-first-order kinetic, pseudo-second-order kinetic, and intra-particle diffusion models.
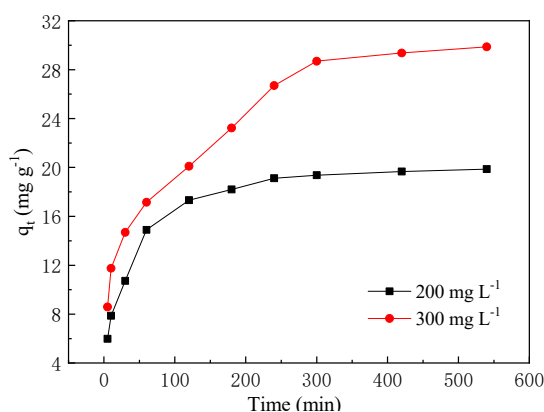

Figure 2. Adsorption kinetics at two different concentrations of Pb(II).

The pseudo-first order kinetic equation [41] is expressed as follows:

$$\log(q_e - q_t) = \log q_e - \frac{k_1}{2.303}t, \tag{16}$$

where q_e and q_t are the amounts of solute adsorbed per unit adsorbent at equilibrium and at any time, respectively (mg g^{-1}), and k_1 is the pseudo-first order rate constant of the adsorption process (min^{-1}).

The pseudo-second order kinetic equation is expressed as follows:

$$\frac{t}{q_t} = \frac{1}{k_2 q_e^2} + \frac{1}{q_e}t, \tag{17}$$

where k_2 is the pseudo-second order rate constant of the adsorption process (g mg^{-1}min^{-1}).

The equation for the intra-particle diffusion model is expressed as follows:

$$q_t = k_i t^{1/2} + C, \tag{18}$$

where k_i is the intra-particle diffusion constant (mg g^{-1} min$^{-1/2}$) and C is the intercept.

The kinetic model parameters of Pb(II) adsorption on BSC are listed in Table 4. The pseudo-second-order kinetic fitting appears to be the best, with correlation coefficients (R^2) of 0.99 and 0.98 for the initial Pb(II) concentrations of 200 mg L^{-1} and 300 mg L^{-1}, respectively. The equilibrium adsorption amounts of Pb(II) calculated using the pseudo-second-order kinetic equation were 20.60 mg g^{-1} and 31.54 mg g^{-1}, respectively, which were consistent with the corresponding experimental results of 19.87 mg g^{-1} and 29.86 mg g^{-1}.

Table 4. Kinetic parameters for adsorption of Pb(II) on BSC.

	C_0 (mg L^{-1})	
	200	300
Pseudo-first order kinetics		
q_e (mg g^{-1})	10.26	24.36
k_1 ($\times 10^{-3}$ min^{-1})	8.75	9.28
R^2	0.96	0.97
Pseudo-second order kinetics		
q_e (mg g^{-1})	20.60	31.54
k_2 ($\times 10^{-3}$g mg^{-1} min^{-1})	2.40	0.83
R^2	0.99	0.98
Intra-particle diffusion model		
k_{i1} (mg g^{-1} min$^{-1/2}$)	1.56	1.46
C_1	2.58	6.24
R_1^2	0.99	0.95
k_{i2} (mg g^{-1} min$^{-1/2}$)	0.46	1.24
C_2	11.74	7.05
R_2^2	0.94	0.99

Furthermore, Figure 3c shows multi-line fitting, indicating that the total rate of adsorption is determined by two stages, namely liquid film diffusion and in-particle diffusion because BSC is a porous medium. In particular, Pb(II) is adsorbed from the liquid phase to BSC through three consecutive steps: First, in the membrane diffusion stage, Pb(II) diffuses to the outer surface of BSC through an imaginary fluid dielectric film. Second, Pb(II) diffuses from the outer surface of BSC to the inner pore of the particle, thus diffusing to the inner surface. Third, in the equilibrium stage, the adsorption reaction is balanced. As can be inferred from the data in Table 3, the diffusion boundary layer thickness in particles (C_2) was greater than that in the liquid film (C_1); therefore, the diffusion rate of the liquid film (k_{i1}) was significantly higher than that in the particles (k_{i2}).
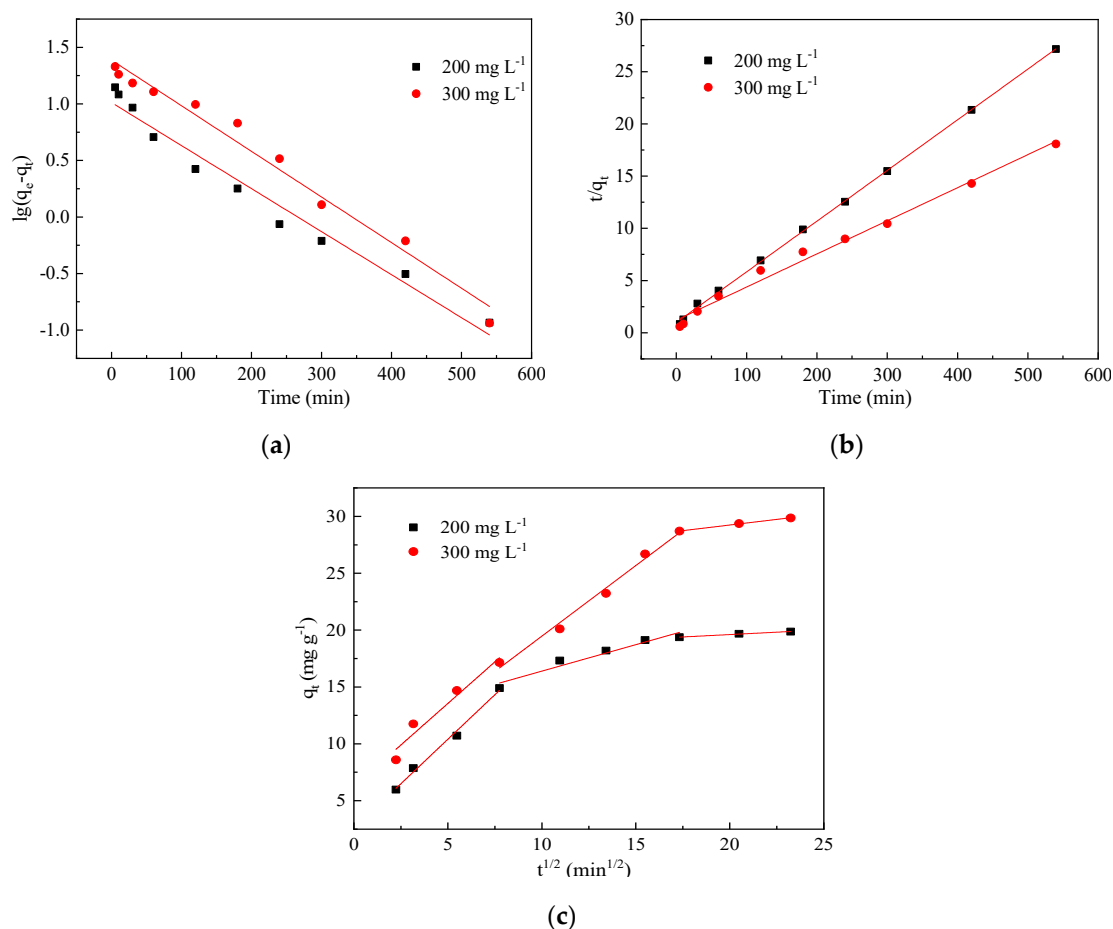
(**a**)

(**b**)

(**c**)

Figure 3. Linearized plots for (**a**) pseudo-first-order kinetics, (**b**) pseudo-second-order kinetics, and (**c**) intra-particle diffusion model of Pb(II) adsorption onto BSC.

3.3. Adsorption Isotherms

Figure 4 shows the isothermal adsorption curves of Pb(II) onto BSC at different temperatures. According to the classification of isothermal adsorption curves by Giles et al. [42], the isothermal adsorption curves showed an "L" shape at reaction temperatures of 278, 288, and 298 K, and an "H" shape at reaction temperatures of 308 and 318 K. The adsorption amount of Pb(II) onto BSC increased with an increase in the concentration of Pb(II). Within the range of the Pb(II) concentrations that we tested for (i.e., 100–600 mg L^{-1}), the adsorption capacity of BSC for Pb(II) did not reach saturation. The Langmuir, Freundlich, D-R, and Brunauer Emmett Teller(BET) models were used to analyze the experimental data to explain the adsorption mechanism of Pb(II) on BSC. The linear plots are shown in Figure 5.
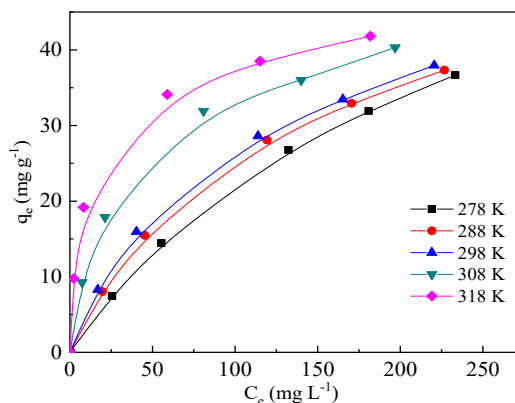
Figure 4. Isotherms of Pb(II) adsorption on BSC.

The Langmuir isotherm model [41] can be expressed as follows:

$$\frac{C_e}{q_e} = \frac{1}{bq_m} + \frac{C_e}{q_m}, \tag{19}$$

where C_e is the equilibrium solute concentration (mg L^{-1}), q_e is the adsorption amount at equilibrium (mg g^{-1}), q_m is the monolayer saturation capacity (mg g^{-1}), and b is the Langmuir constant (L mg^{-1}).

The Freundlich isotherm model can be expressed as follows:

$$\ln q_e = \ln K_F + \frac{1}{n} \ln C_e, \tag{20}$$

where C_e and q_e are defined in the same manner as in Equation (19), K_F is the Freundlich constant (L g^{-1}) indicating the adsorption capacity, and n is the isotherm constant indicating the adsorption intensity.

The D-R model can be expressed as follows:

$$\ln q_e = \ln q_m - k\varepsilon^2, \tag{21}$$

where q_m is the monolayer saturation capacity (mol g^{-1}), k is the model constant of adsorption energy (mol^2 kJ^{-2}), and ε is the Polanyi potential, which is given by:

$$\varepsilon = RT \ln(1 + \frac{1}{C_e}), \tag{22}$$

where the unit for E should in mol L^{-1}.

The mean free energy of adsorption E is:

$$E = -\frac{1}{\sqrt{2k}}, \tag{23}$$

In general, adsorption is attributed to surface adsorption by means of ion exchange when |E| is between 8.0 and 16.0 kJ mol^{-1}, while to physical adsorption when |E| is between 1.0 and 8.0 kJ mol^{-1}.

The BET model can be expressed as follows

$$\frac{C_e}{(C_s - C_e)q_e} = \frac{1}{Bq_0} + \frac{B-1}{Bq_0}\frac{C_e}{C_s}, \tag{24}$$

where C_e and q_e are defined in the same manner as in Equation (19), q_0 is the monolayer saturation capacity (g g^{-1}), C_s is the saturated concentration of the adsorbate (g L^{-1}), and B is the BET constant.
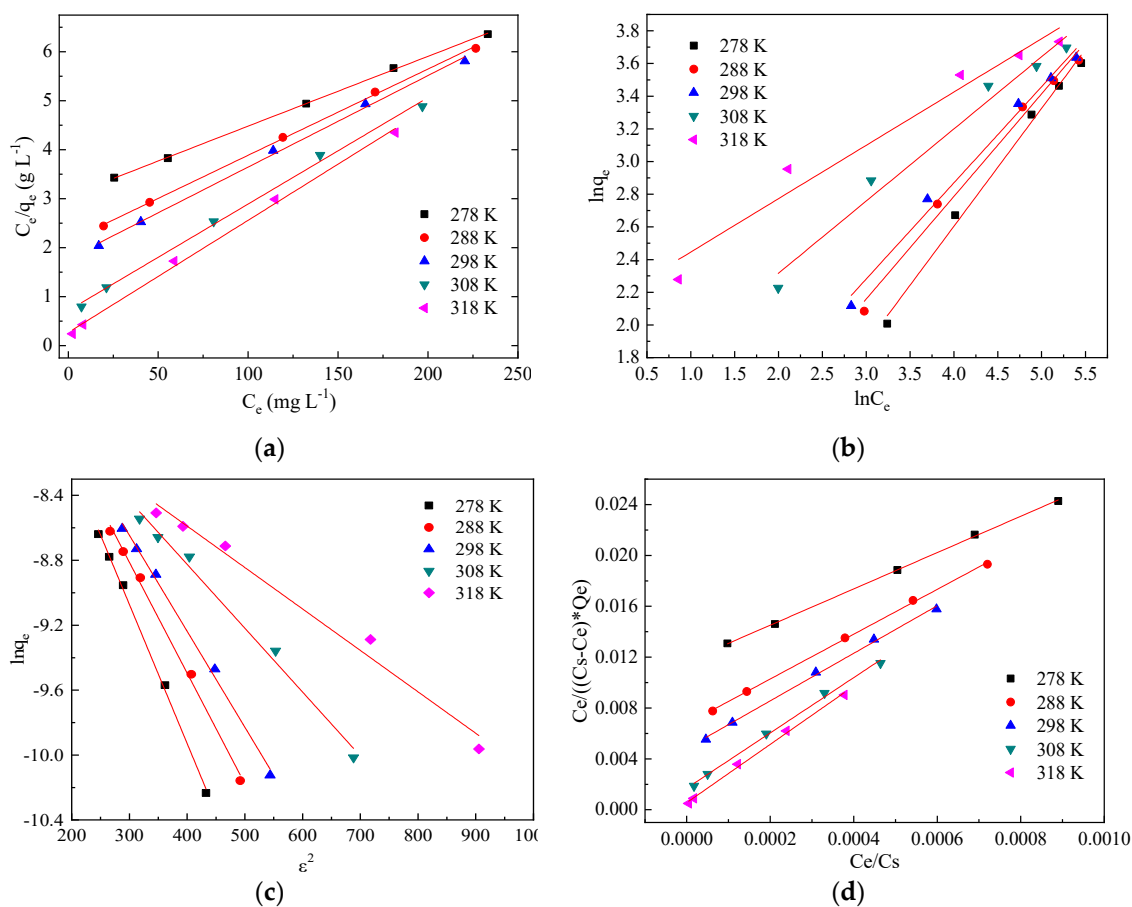
Figure 5. Linear plots of (**a**) Langmuir isotherm, (**b**) Freundlich isotherm, (**c**) D-R model, and (**d**) BET model for Pb(II) adsorption onto BSC.

It can be seen from Table 5 that the fitting effect of the four isothermal models is good, and the correlation coefficients of Langmuir and BET models are relatively high, indicating that Langmuir and BET models are more suitable to describe the isothermal adsorption process of Pb(II) onto BSC than the other models. It should be noted that the adsorption of Pb(II) by bentonite satisfied the Langmuir model. In addition, the alkalinity released by BSC reacts with Pb(II) to form a hydroxide, which accumulates layer by layer on BSC, which continues to adsorb Pb(II). A synergistic adsorption–coagulation effect occurs, leading to the appearance of multiple layers locally on the surface of BSC, which satisfies the BET model.

Table 5. Isothermal constants for the adsorption of Pb(II) onto BSC at different temperatures.

	278 K	288 K	298 K	308 K	318 K
Langmuir isotherm					
q_m (mg g^{-1})	43.63	45.99	53.53	56.79	70.18
b (L mg^{-1})	0.0047	0.0083	0.0105	0.0303	0.0856
R^2	0.999	0.999	0.997	0.995	0.996
Freundlich isotherm					
K_F (L g^{-1})	0.76	1.32	1.68	4.19	8.33
n	1.39	1.59	1.69	2.27	3.06
R^2	0.992	0.987	0.986	0.971	0.955

Table 5. *Cont.*

D–R isotherm					
q_m (mg g^{-1})	107.06	146.99	214.69	238.96	310.42
k (mol^2 kJ^{-2})	0.0085	0.0068	0.0059	0.0039	0.0025
E (kJ mol^{-1})	−7.64	−8.56	−9.19	−11.27	−13.99
R^2	0.997	0.995	0.995	0.986	0.977
BET isotherm					
q_0 (mg g^{-1})	43.61	45.97	53.46	56.69	70.00
R^2	0.999	0.999	0.997	0.995	0.996

When the temperature was increased from 278 to 318 K in increments of 10 K, the monolayer saturated adsorption capacities calculated via the Langmuir isothermal model were 43.63, 45.99, 53.53, 56.79 and 70.18 mg g^{-1}, respectively, which was, in essence, the same as that calculated using the BET model. Thus, it was verified that the adsorption of Pb(II) on BSC satisfied the Langmuir and BET models.

Using the Freundlich model, n was calculated to be greater than 1, indicating that the adsorption process was spontaneous. However, when the temperature was 308 K and 318 K, n was greater than 2, indicating that adsorption was spontaneous and easier. These results proved that the adsorption of Pb(II) by BSC was an endothermic process, and the increase of temperature was beneficial to the adsorption of Pb(II) by BSC. For the same set of temperatures as above, the saturated adsorption capacities calculated using the D-R model were 107.06, 146.99, 214.69, 238.96, and 310.42 mg g^{-1}, respectively. It can be observed that, at the same temperature, the saturated adsorption capacity obtained using the D-R model was larger than that obtained using the Langmuir model; this is because the D-R model assumed an ideal state in which all micropores were filled with Pb(II), which was difficult to achieve in practice. Furthermore, when the temperature was increased from 278 to 318 K in increments of 10 K, the average free energy of adsorption (E) was −7.64, −8.56, −9.19, −11.27, and −13.99, respectively, indicating that the adsorption process at the four temperatures other than 278 K was dominated by ion exchange, compared with physical adsorption at 278 K.

3.4. Adsorption Thermodynamics

The thermodynamic [43] behavior of Pb(II) adsorption on BSC was evaluated using the following equations:

$$\Delta G^0 = -RT \ln K_c, \tag{25}$$

$$\Delta G^0 = \Delta H^0 - T\Delta S^0, \tag{26}$$

where K_c is the distribution coefficient of the solute between adsorbent and solution in equilibrium (q_e/C_e), R the air constant, T is the temperature (K), ΔH^0 is the change of enthalpy, ΔS^0 is the change of entropy, and ΔG^0 the standard Gibb's free energy.

Equations (25) and (26) can be written in a linearized form between $\ln(K_c)$ and $1/T$ as follows:

$$\ln(K_c) = \frac{\Delta S^0}{R} - \frac{\Delta H^0}{RT}, \tag{27}$$

Figure 6 is the line fitted according to the linear equation between ln Kc and 1/T, the values of ΔH^0 and ΔS^0 can be calculated from the intercept and slope of the plots. Table 6 lists the thermodynamic parameters of Pb(II) adsorption on BSC. When the concentration of Pb(II) is unchanged, the Gibb's free energy decreased with an increase of temperature and is all negative, indicating that the adsorption reaction of BSC to Pb(II) is spontaneous; it should be noted that the higher the temperature, the stronger the spontaneity. In contrast, with an increase in the concentration of Pb(II), ΔH^0 decreases and is all positive, indicating that adsorption reaction is an endothermic process. Furthermore, when the concentration of Pb(II) was increased from 100 mg L^{-1} to 600 mg L^{-1}, all ΔS^0 values were positive,

but decreased from 141.84 J mol^{-1}K^{-1} to 9.94 J mol^{-1}K^{-1}, indicating that the degree of freedom of the Pb(II)-BSC system increased with the adsorption reaction; in particular, the higher the initial concentration of Pb(II), the greater the disorder degree of the system.
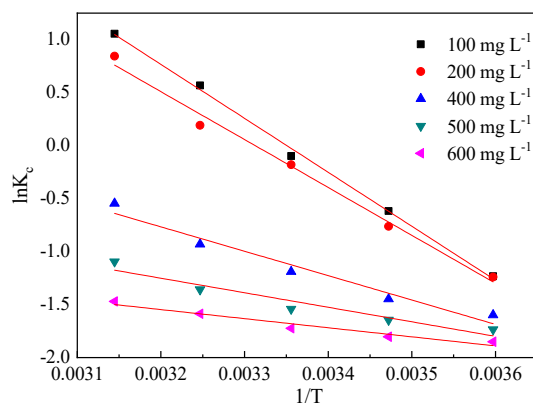

Figure 6. Van't Hoff plots for Pb(II) adsorption onto BSC.

**Table 6.** Thermodynamic parameters for the adsorption of Pb(II) on BSC.

C_0 (mg L^{-1})	T (K)	ΔG^0 (kJ mol^{-1})	ΔH^0 (kJ mol^{-1})	ΔS^0 (J mol^{-1}K^{-1})	R
100	278	−5.41	34.02	141.84	0.997
	288	−6.83			
	298	−8.25			
	308	−9.67			
	318	−11.09			
200	278	−5.34	29.27	124.51	0.988
	288	−6.59			
	298	−7.83			
	308	−9.08			
	318	−10.32			
400	278	−4.43	10.82	54.84	0.951
	288	−4.98			
	298	−5.53			
	308	−6.08			
	318	−6.62			
500	278	−2.50	4.75	26.07	0.905
	288	−2.76			
	298	−3.02			
	308	−3.28			
	318	−3.54			
600	278	−1.46	1.31	9.94	0.937
	288	−1.56			
	298	−1.65			
	308	−1.76			
	318	−1.85			

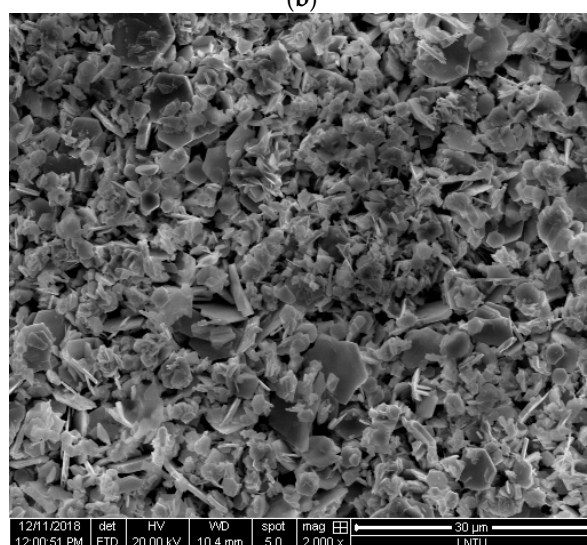*3.5. Microstructure Characterization Results*

Figure 7 shows the SEM images of the BSC before the reaction, BSC after the reaction, and precipitate generated after the reaction. BSC before the reaction exhibits an uneven surface and large pores, which are conducive to ion absorption, alkalinity release, and sediment accumulation. On the surface of the BSC after the reaction, there are dense clusters of aggregates, and many small pores have generated, possibly due to the continuous accumulation of sediments. These small pores can continue to facilitate adsorption. The sediment formed after the reaction is larger than the particles of the BSC after the reaction, in the form of loose large flakes or needles.
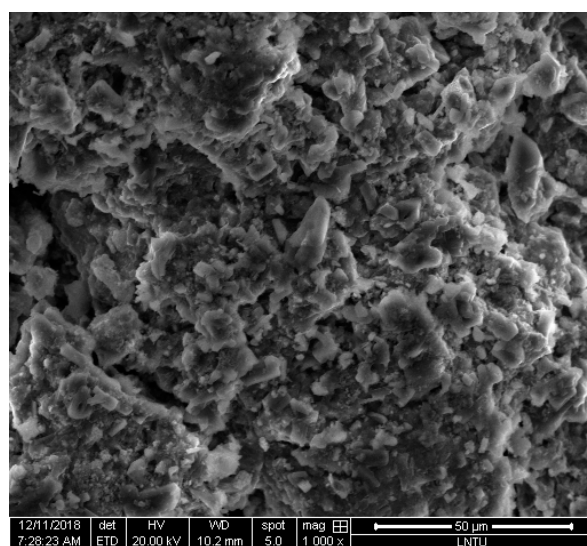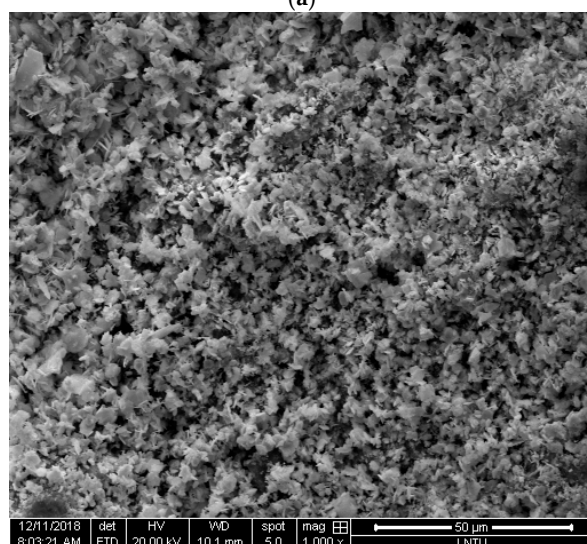
Figure 7. SEM images of (a) BSC before reaction, (b) BSC after reaction, and (c) precipitation after reaction.

Figure 8 shows the XRD patterns of the BSC before the reaction, BSC after the reaction, and the precipitate generated after the reaction. According to (a), the mineral phases of BSC before the reaction are mainly $CaCO_3$, SiO_2, $Na_2AlSi_3O_8OH$, and Ca_2SiO_4, which are the main components of calcite, quartz, bentonite, and steel slag respectively. According to (b), the main mineral phases of BSC after the reaction are $CaCO_3$, SiO_2, PbO, PbO_2, Pb_2O_3, Pb_2SiO_4, Pb_4SiO_6, $Pb_5Si_4O_8(OH)_{10}$, Ca_2PbO_4, and Na_6PbO_5. This indicates that $CaCO_3$ and SiO_2 do not change during the reaction, while the other phases are new minerals generated during Pb removal. BSC releases Ca^{2+}, Na^+, and OH^- ions in solution. PbO, PbO_2, and Pb_2O_3 are generated by the thermal decomposition of $Pb(OH)_2$ generated by the reaction of Pb^{2+} and OH^- ions; Pb_2SiO_4 and Pb_4SiO_6 are generated by the electrostatic adsorption of Pb^{2+} and silicate on BSC; $Pb_5Si_4O_8(OH)_{10}$ is generated by Pb^{2+}, OH^-, and silicate ions; and Ca_2PbO_4 and Na_6PbO_5 are generated by the thermal decomposition of compounds generated by Ca^{2+}, Na^+, Pb^{2+}, and OH^- reactions. According to (c), the reaction precipitates are mainly $PbCO_3$, $Pb_4(SO_4)(CO_3)_2(OH)_2$, $Pb_3(CO_3)_2(OH)_2$, and $Pb_3(CO_2)_2(OH)_2$. When in contact with water, BSC will release CO_3^{2-}, SO_4^{2-}, and OH^- ions into the solution, where $PbCO_3$ is generated by the electrostatic adsorption of Pb^{2+} and CO_3^{2-}. $Pb_4(SO_4)(CO_3)_2(OH)_2$, $Pb_3(CO_3)_2(OH)_2$, and $Pb_3(CO_2)_2(OH)_2$ are complexes formed by coordination between Pb^{2+}, CO_3^{2-}, SO_4^{2-}, and OH^-.

(a)

(b)
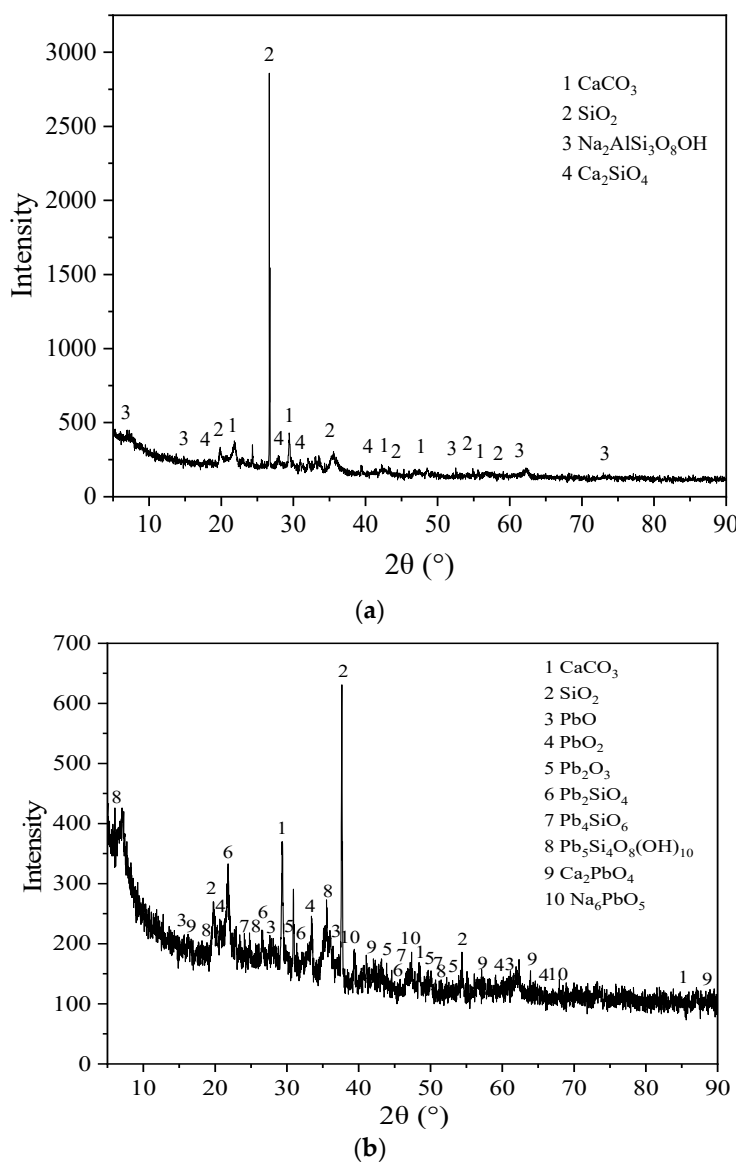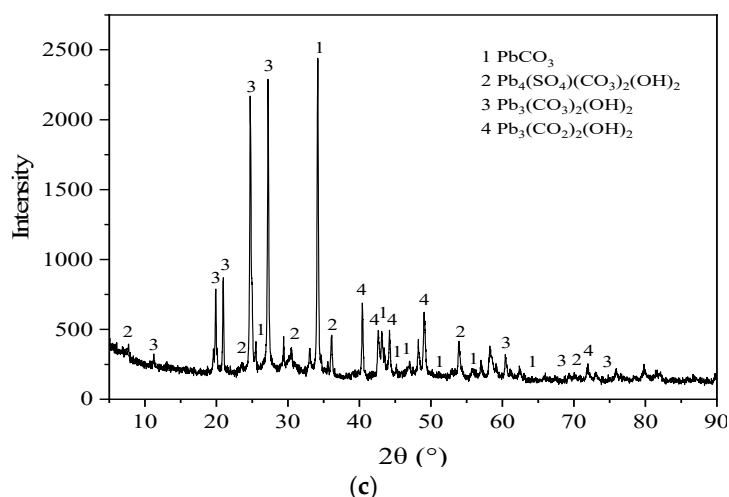
Figure 8. *Cont.*

Figure 8. XRD patterns of (**a**) BSC before reaction, (**b**) BSC after reaction, and (**c**) precipitation after reaction.

4. Conclusions

In this study, the adsorption behavior of Pb(II) onto BSC was studied, thus providing a theoretical basis for AMD treatment containing Pb(II). First, we observed that the dependence of the adsorption process on pH was similar to that of the formation of soluble and insoluble hydrolysates of Pb(II) on the pH value. The adsorption mechanism included ion exchange, complexation, precipitation, and a synergistic adsorption–coagulation effect. Hydrolysis and precipitation of Pb(II), as well as the interactions between Pb(II) and minerals and slag glass in BSC, were expressed by equations. Second, the pseudo-first-order kinetic, pseudo-second-order kinetic, and intra-particle diffusion models were used to fit the kinetic data. The pseudo-second-order kinetic model was the most suitable to describe the adsorption kinetics of Pb(II) onto BSC. In addition, it was observed that the total adsorption rate was controlled by liquid film diffusion and intra-particle diffusion. Third, the isothermal adsorption data were analyzed using the Langmuir, Freundlich, D-R, and BET models. The Langmuir and BET models led to the best isotherms. Fourth, thermodynamic analysis revealed that the adsorption process was spontaneous and endothermic, and that the degree of freedom of the Pb(II)-BSC system increased with time. Lastly, the BSC before and after the reaction, as well as the precipitation after the reaction, were characterized by SEM and XRD. In this study, the kinetic, isothermal adsorption, thermodynamic properties, mechanism, and microscopic characterization of Pb(II) adsorption on BSC were studied. The results offer further scope to study the desorption behaviors and to perform dynamic experiments. Therefore, to conclude, BSC is a good adsorbent for treating Pb(II)- containing AMD. It is a new multifunctional mineral material that allows neutralization, adsorption, coagulation, and filtration.

References

1. Kefeni, K.K.; Msagati, T.A.M.; Mamba, B.B. Acid mine drainage: Prevention, treatment options, and resource recovery: A review. *J. Clean. Prod.* **2017**, *151*, 475–493. [CrossRef]

2. Qin, W.J.; Han, D.M.; Song, X.F.; Engesgaard, P. Effects of an abandoned Pb-Zn mine on a karstic groundwater reservoir. *J. Geochem. Explor.* **2019**, *200*, 221–233. [CrossRef]

3. Balistrieri, L.S.; Seal, R.R.; Piatak, N.M.; Paul, B. Assessing the concentration, speciation, and toxicity of dissolved metals during mixing of acid-mine drainage and ambient river water downstream of the Elizabeth Copper Mine, Vermont, USA. *Appl. Geochem.* **2007**, *22*, 930–952. [CrossRef]

4. Beygli, R.A.; Mohaghegh, N.; Rahimi, E. Metal ion adsorption from wastewater by g-C3N4 modified with hydroxyapatite: A case study from Sarcheshmeh Acid Mine Drainage. *Res. Chem. Intermediat.* **2019**, *45*, 2255–2268. [CrossRef]

5. Gutierrez, M.; Mickus, K.; Camacho, L.M. Abandoned Pb-Zn mining wastes and their mobility as proxy to toxicity: A review. *Sci. Total Environ.* **2016**, *565*, 392–400. [CrossRef] [PubMed]

6. Oldham, C.; Beer, J.; Blodau, C.; Fleckenstein, J.; Jones, L.; Neumann, C.; Peiffer, S. Controls on iron(II) fluxes into waterways impacted by acid mine drainage: A Damkohler analysis of groundwater seepage and iron kinetics. *Water Res.* **2019**, *153*, 11–20. [CrossRef] [PubMed]

7. Sephton, M.G.; Webb, J.A. The role of secondary minerals in remediation of acid mine drainage by Portland cement. *J. Hazard. Mater.* **2019**, *367*, 267–276. [CrossRef]

8. Mamelkina, M.A.; Tuunila, R.; Sillanpaa, M.; Hakkinen, A. Systematic study on sulfate removal from mining waters by electrocoagulation. *Sep. Purif. Technol.* **2019**, *216*, 43–50. [CrossRef]

9. Aguiar, A.O.; Andrade, L.H.; Ricci, B.C.; Pires, W.L.; Miranda, G.A.; Amaral, M.C.S. Gold acid mine drainage treatment by membrane separation processes: An evaluation of the main operational conditions. *Sep. Purif. Technol.* **2016**, *170*, 360–369. [CrossRef]

10. Vital, B.; Bartacek, J.; Ortega-Bravo, J.C.; Jeison, D. Treatment of acid mine drainage by forward osmosis: Heavy metal rejection and reverse flux of draw solution constituents. *Chem. Eng. J.* **2018**, *332*, 85–91. [CrossRef]

11. Bai, H.; Kang, Y.; Quan, H.E.; Han, Y.; Sun, J.; Feng, Y. Treatment of acid mine drainage by sulfate reducing bacteria with iron in bench scale runs. *Bioresour. Technol.* **2013**, *128*, 818–822. [CrossRef] [PubMed]

12. Yildiz, M.; Yilmaz, T.; Arzum, C.S.; Yurtsever, A.; Kaksonen, A.H.; Ucar, D. Sulfate reduction in acetate- and ethanol-fed bioreactors: Acidic mine drainage treatment and selective metal recovery. *Miner. Eng.* **2019**, *133*, 52–59. [CrossRef]

13. Pat-Espadas, A.M.; Portales, R.L.; Amabilis-Sosa, L.E.; Gomez, G.; Vidal, G. Review of Constructed Wetlands for Acid Mine Drainage Treatment. *Water* **2018**, *10*, 1685. [CrossRef]

14. Park, I.; Tabelin, C.B.; Jeon, S.; Li, X.L.; Seno, K.; Ito, M.; Hiroyoshi, N. A review of recent strategies for acid mine drainage prevention and mine tailings recycling. *Chemosphere* **2019**, *219*, 588–606. [CrossRef] [PubMed]

15. Alakangas, L.; Andersson, E.; Mueller, S. Neutralization/prevention of acid rock drainage using mixtures of alkaline by-products and sulfidic mine wastes. *Environ. Sci. Pollut. Res.* **2013**, *20*, 7907–7916. [CrossRef] [PubMed]

16. Madzivire, G.; Maleka, P.P.; Vadapalli, V.R.K.; Gitari, W.M.; Lindsay, R.; Petrik, L.F. Fate of the naturally occurring radioactive materials during treatment of acid mine drainage with coal fly ash and aluminium hydroxide. *J. Environ. Manag.* **2014**, *133*, 12–17. [CrossRef] [PubMed]

17. Zuo, Q.; Zhang, Y.; Zheng, H.; Zhang, P.Y.; Yang, H.W.; Yu, J.; Tang, J.; Zheng, Y.D.; Mai, J.J. A facile method to modify activated carbon fibers for drinking water purification. *Chem. Eng. J.* **2019**, *65*, 175–182. [CrossRef]

18. Mohan, D.; Pittman, C.U. Activated carbons and low cost adsorbents for remediation of triand hexavalent chromium from water. *J. Hazard. Mater.* **2006**, *137*, 762–811. [CrossRef]

19. Li, H.; Zhou, M.; Han, Y.; Shi, B.C.; Xiong, Q.; Hou, H.B. Mechanism of red mud combined with steel slag conditioning for sewage sludge dewatering. *Desalin. Water Treat.* **2018**, *135*, 133–140. [CrossRef]

20. Liu, L.; Yu, L.J.; Zhang, W.; Fan, J.H.; Zuo, Q.T.; Li, M.J.; Yan, Z.F.; You, Z.C.; Wang, R.Y. Adsorption performance of Pb(II) ions from aqueous solution onto a novel complex of coffee grounds and attapulgite clay. *Desalin. Water Treat.* **2019**, *153*, 208–215. [CrossRef]

21. Li, Z.Y.; Pan, Z.D.; Wang, Y.M. Enhanced adsorption of cationic Pb(II) and anionic Cr(VI) ions in aqueous solution by amino-modified nano-sized illite-smectite clay. *Environ. Sci. Pollut. Res.* **2019**, *26*, 11126–11139. [CrossRef]

22. Sun, L.M.; Wang, J.S.; Wu, J.S.; Wang, T.N.; Du, Y.C.; Li, Y.L.; Li, H.Y. Constructing nanostructured silicates on diatomite for Pb(II) and Cd(II) removal. *J. Mater. Sci.* **2019**, *54*, 6882–6894. [CrossRef]

23. Ciosek, A.L.; Luk, G.K. Kinetic Modelling of the Removal of Multiple Heavy Metallic Ions from Mine Waste by Natural Zeolite Sorption. *Water* **2017**, *9*, 482. [CrossRef]

24. Tomasz, K.; Anna, K.; Ryszard, C. Effective adsorption of lead ions using fly ash obtained in the novel circulating fluidized bed combustion technology. *Microchem. J.* **2019**, *145*, 1011–1025. [CrossRef]

25. Koz, B.; Cevik, U. Lead adsorption capacity of some moss species used for heavy metal analysis. *Ecol. Indic.* **2014**, *36*, 491–494. [CrossRef]

26. Dizadji, N.; Anaraki, N.A. Adsorption of chromium and copper in aqueous solutions using tea residue. *Int. J. Environ. Sci. Technol.* **2011**, *8*, 631–638. [CrossRef]

27. Da Gama, B.M.V.; Do Nascimento, G.E.; Sales, D.C.S.; Rodriguez-Diaz, J.M.; Barbosa, C.M.B.D.; Duarte, M.M.M.B. Mono and binary component adsorption of phenol and cadmium using adsorbent derived from peanut shells. *J. Clean. Prod.* **2018**, *201*, 219–228. [CrossRef]

28. Amin, M.T.; Alazba, A.A.; Shafiq, M. Adsorptive Removal of Reactive Black 5 from Wastewater Using Bentonite Clay: Isotherms, Kinetics and Thermodynamics. *Sustainability* **2015**, *7*, 15302–15318. [CrossRef]

29. Mohajeri, P.; Smith, C.; Selamat, M.R.; Aziz, H.A. Enhancing the Adsorption of Lead (II) by Bentonite Enriched with pH-Adjusted Meranti Sawdust. *Water* **2018**, *10*, 1875. [CrossRef]

30. Deng, G.R.; Ma, J.C.; Zhang, X.P.; Zhang, Q.F.; Xiao, Y.Q.; Ma, Q.L.; Wang, S.B. Magnetic natural composite Fe3O4-chitosan@bentonite for removal of heavy metals from acid mine drainage. *J. Colloid Interface Sci.* **2019**, *538*, 132–141.

31. Tsai, T.T.; Kao, C.M.; Wang, J.Y. Remediation of TCE-contaminated groundwater using acid/BOF slag enhanced chemical oxidation. *Chemosphere* **2011**, *83*, 687–692. [CrossRef]

32. Molahid, V.L.M.; Kusin, F.M.; Madzin, Z. Role of multiple substrates (spent mushroom compost, ochre, steel slag, andlimestone) in passive remediation of metal-containing acid mine drainage. *Environ. Technol.* **2019**, *40*, 1323–1336. [CrossRef]

33. Reddy, K.R.; Gopakumar, A.; Chetri, J.K. Critical review of applications of iron and steel slags for carbon sequestration and environmental remediation. *Rev. Environ. Sci. Bio Technol.* **2019**, *18*, 127–152. [CrossRef]

34. Xiao, L.P.; Liu, Z.; Bai, J.C.; Luan, X.F.; Li, Y.; Wei, B. Zn2+ removal mechanism by bentonite-steel slag composite particles. *J. China Coal Soc.* **2017**, *42*, 1005–1012.

35. Naidu, G.; Ryu, S.; Thiruvenkatachari, R.; Choi, Y.; Jeong, S.; Vigneswaran, S. A critical review on remediation, reuse, and resource recovery from acid mine drainage. *Environ. Pollut.* **2019**, *247*, 1110–1124. [CrossRef]

36. Yuan, L.; Liu, Y.S. Removal of Pb(II) and Zn(II) from aqueous solution by ceramisite prepared by sintering bentonite, iron powder and activated carbon. *Chem. Eng. J.* **2013**, *215*, 432–439. [CrossRef]

37. Chen, G.N.; Shah, K.J.; Shi, L.; Chiang, P.C. Removal of Cd(II) and Pb(II) ions from aqueous solutions by synthetic mineral adsorbent: Performance and mechanisms. *Appl. Surf. Sci.* **2017**, *409*, 296–305. [CrossRef]

38. Dimitrova, S.V.; Mehandgiev, D.R. Lead removal from aqueous solutions by granulated blast-furnace slag. *Water Res.* **1998**, *32*, 3289–3292. [CrossRef]

39. Zhao, D.L.; Sheng, G.D.; Hu, J. The adsorption of Pb(II) on Mg2Al layered double hydroxide. *Chem. Eng. J.* **2011**, *171*, 167–174. [CrossRef]

40. Wang, S.W.; Dong, Y.H.; He, M.L. Characterization of GMZ bentonite and its application in the adsorption of Pb(II) from aqueous solutions. *Appl. Clay Sci.* **2009**, *43*, 164–171. [CrossRef]

41. Wang, Y.; Tang, X.W.; Chen, Y.M.; Zhan, L.T.; Li, Z.Z.; Tang, Q. Adsorption behavior and mechanism of Cd(II) on loess soil from China. *J. Hazard. Mater.* **2009**, *172*, 30–37. [CrossRef]

42. Giles, C.H.; Smith, D.; Huitson, A. General treatment and classification of solute adsorption- isotherms. I. Theoretical. *J. Colloid Interface Sci.* **1974**, *47*, 755–765. [CrossRef]

43. Tang, X.W.; Li, Z.Z.; Chen, Y.M.; Wang, Z.Q. Removal of Zn(II) from aqueous solution with natural Chinese loess: Behaviors and affecting factors. *Desalination* **2009**, *249*, 49–57. [CrossRef]